Binding energies of exciton complexes in transition metal dichalcogenide monolayers and effect of dielectric environment

Ilkka Kylänpää[1] and Hannu-Pekka Komsa[2]
[1]*Department of Physics, Tampere University of Technology, P.O. Box 692, FI-33101 Tampere, Finland*
[2]*COMP, Department of Applied Physics, Aalto University, P.O. Box 11100, 00076 Aalto, Finland*
(Received 10 August 2015; revised manuscript received 16 October 2015; published 16 November 2015)

Excitons, trions, biexcitons, and exciton-trion complexes in two-dimensional transition metal dichalcogenide sheets of MoS_2, $MoSe_2$, $MoTe_2$, WS_2, and WSe_2 are studied by means of density functional theory and path-integral Monte Carlo method in order to accurately account for the particle-particle correlations. In addition, the effect of dielectric environment on the properties of these exciton complexes is studied by modifying the effective interaction potential between particles. Calculated exciton and trion binding energies are consistent with previous experimental and computational studies, and larger systems such as biexciton and exciton-trion complex are found highly stable. Binding energies of biexcitons are similar to or higher than those of trions, but the binding energy of the trion depends significantly stronger on the dielectric environment than that of biexciton. Therefore, as a function of an increasing dielectric constant of the environment the exciton-trion complex "dissociates" to a biexciton rather than to an exciton and a trion.

DOI: 10.1103/PhysRevB.92.205418 PACS number(s): 73.22.Lp, 71.35.−y, 71.10.Li

I. INTRODUCTION

Layered transition metal dichalcogenides (TMDs) are chemically, thermally, and mechanically stable even in the monolayer form, and thus, provide an ideal platform for studying condensed-matter physics in two dimensions. The semiconducting TMDs present many unusual optical properties such as strong excitonic effects [1], valley-dependent circular dichroism [2], and second-harmonic generation [3], whose magnitude depends sensitively on the number of layers. For instance, the prototypical MoS_2 material is a semiconductor with 1.1-eV indirect band gap in bulk, but 1.9-eV direct band gap in the monolayer [1]. Importantly, the reduced dimensionality is manifested in a large exciton binding energy of 0.5–1 eV, but also of significant binding energy in the case of charged excitons, or trions, consisting of three charge carriers. This suggests that even larger complexes might be stable. Indeed, experimental reports assigned to biexciton formation have very recently appeared in the literature [4–6].

Theoretical studies are invaluable in predicting the stability of these complexes and in interpreting the experimental results. Excitons can be calculated reliably from first principles by solving the Bethe-Salpeter equation (BSE) on top of quasiparticle band structure. Binding energies have also been calculated using simple variational or tight-binding models based on an effective 2D interaction potential and the effective mass approach [6–13], yielding fairly good agreement with experiments and with the BSE results in the case of excitons. This has also raised interest to apply similar approaches to study larger exciton complexes [6,14], in comparison to the theoretical estimates based on quantum well systems [4,15,16].

Difficulties in constructing a reasonable wave-function ansatz in the case of the larger complexes hinders straightforward extension of the simple variational models. Within the effective mass approach, quantum Monte Carlo (QMC) methods, such as diffusion Monte Carlo and path integral Monte Carlo (PIMC), provide accurate and powerful means for studying few-particle systems [17–19]. The main advantage in QMC methods is the exact account of particle-particle correlations, which is particularly important in an accurate description of exciton complexes. To this end, we utilize the PIMC method, which is a basis set free approach for solving finite temperature quantum statistics.

Although two-dimensional (2D) materials are not directly bonded with the environment, due to their thinness, they are highly sensitive to electromagnetic fields, doping, or dielectric screening of their surroundings. In particular, the Coulomb interaction between an electron and a hole in an exciton is screened by the dielectric environment and the binding energy changes dramatically [10–12,20–22]. It is rather surprising then that the effect of the dielectric environment on the binding energy of trions, let alone on the larger complexes, has been rarely investigated [14].

Here, we present the results from PIMC simulations for exciton, trion, biexciton, and exciton-trion complexes for a set of the most common layered TMD materials: MoS_2, $MoSe_2$, $MoTe_2$, WS_2, and WSe_2. We focus on the binding energies and mean particle distances. Our approach is based on the effective 2D interaction and effective masses, for which relevant parameters are calculated using density functional theory (DFT). In addition, the effect of environment is accounted for in the interaction potential, which allows us to demonstrate the effect of the surroundings to the binding energies and mean distances.

II. METHODS

The geometry of the system is schematically shown in Fig. 1. The electrons and holes are confined to the 2D sheet placed on top of a substrate. We consider two-dimensional many-body Hamiltonians where the interaction potential between charged particles is given as in Refs. [9,10,23],

$$V(r_{ij}) = \frac{q_i q_j \pi}{2\kappa r_*}\left[H_0\left(\frac{r_{ij}}{r_*}\right) - Y_0\left(\frac{r_{ij}}{r_*}\right)\right], \qquad (1)$$

where H_0 and Y_0 are the Struve function and the Bessel function of the second kind, respectively, q_i represents the charge of the particle (here $q_i = e$ or $q_i = -e$). The length

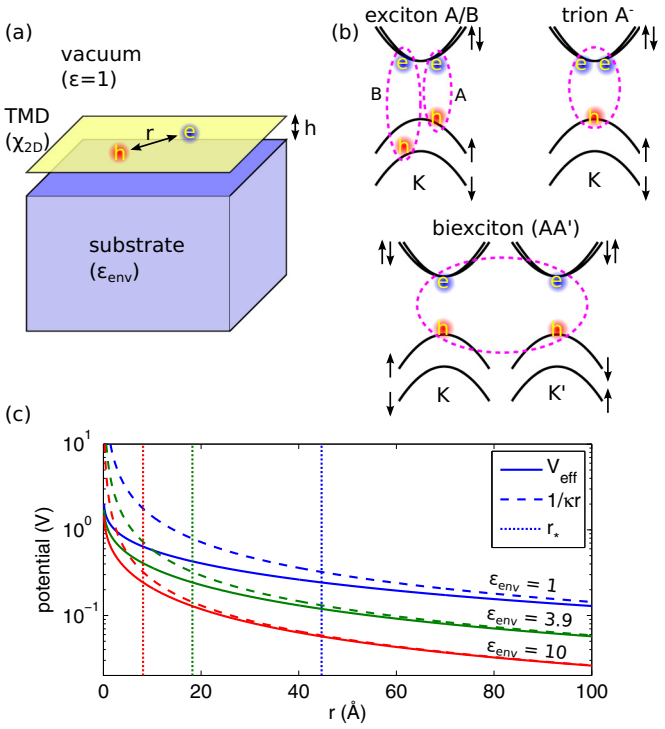

FIG. 1. (Color online) (a) Schematic illustration of the system geometry. (b) Illustration of the exciton, trion, and biexciton systems constructed from the electrons on the conduction band and holes in the valence band. (c) Effective interaction potential in the case of $\varepsilon_{\rm env} = 1$, 3.9 (silica), and 10 (sapphire), as compared to Coulomb interaction in homogeneous system scaled by κ.

scale in the presence of dielectric environment is given as

$$r_* = 2\pi\,\chi_{\rm 2D}/\kappa. \qquad (2)$$

$\chi_{\rm 2D}$ is the 2D polarizability of the sheet [8,9], which can be evaluated from the bulk in-plane dielectric constant $\varepsilon_{||}$ and the layer separation d_s (here half of the perpendicular lattice constant since all considered materials have two layers within the primitive cell): $\chi_{\rm 2D} = d_s(\varepsilon_{||} - 1)/4\pi$. κ is the average dielectric constant of the environment. Here we consider the experimentally most relevant case of TMD sheet placed on a substrate of dielectric constant $\varepsilon_{\rm env}$ and vacuum or air on the other side, in which case $\kappa = (1 + \varepsilon_{\rm env})/2$. The interaction potentials for three representative values of κ in Fig. 1(c) show strong screening by the 2D sheet at short distances and approaching $1/\kappa r$ at $r \gtrsim r_*$. We note that this type of potential is only valid when $\kappa < \varepsilon_{||}$ [24].

The four considered exciton complexes are illustrated in Fig. 1(b). In monolayer TMDs, due to the spin-orbit coupling and the lack of inversion symmetry, the valence-band maximum (VBM) at the K point is split into two bands with distinct spin orientation. The spins are further coupled to the valley index (K or K'). Thus, if the many-body system is supposed to have two holes of opposite spins in the topmost valence-band state, they must be located in different valleys. The conduction-band minimum (CBM) is nearly degenerate (here assumed degenerate) and there is no such restriction for the electrons.

For the model interaction potential two material specific parameters are then needed: polarizability of the sheet and the effective masses of electrons and holes. Both of these quantities can be obtained quite reliably from DFT calculations. Our calculated numbers are collected in Table I. The atomic structures are optimized using revB86b-DF2 functional [25], which yields structural parameters in very good agreement with the experiment [26]. Using these structures, the effective masses and dielectric constants are then calculated using the PBE functional. Bulk dielectric constants are calculated using density functional perturbation theory. Since all materials considered here have direct gap with VBM and CBM located at the K point (in the monolayer form), the effective masses are obtained from the monolayer structure by fitting parabolas to the K valley and accounting for the spin-orbit coupling [24].

TABLE I. Material parameters needed for the effective-mass theory description of the exciton complexes. Layer separation d_s, and $\chi_{\rm 2D}$ are in Å. The two values for m_h correspond to the two spin-orbit split valence bands at K (first for the highest band). ε is dielectric constant in directions parallel to the plane and normal to the plane.

Material	d_s	m_h	m_e	ε	$\chi_{\rm 2D}$
MoS_2	6.180	$-0.54/-0.61$	0.47	15.46/6.46	7.112
$MoSe_2$	6.527	$-0.59/-0.69$	0.55	17.29/7.95	8.461
$MoTe_2$	7.054	$-0.62/-0.75$	0.57	21.87/11.02	11.715
WS_2	6.219	$-0.35/-0.49$	0.32	13.92/5.98	6.393
WSe_2	6.575	$-0.36/-0.53$	0.34	15.47/7.22	7.571

The path-integral Monte Carlo simulations are carried out at $T = 10$ K using the effective-mass approach with the masses obtained from our DFT calculations, and the effective interaction potential given in Eq. (1). Apart from the exciton-trion complex we can consider our particles as "boltzmannons," i.e., they obey the Boltzmann statistics and are treated as distinguishable particles. In the case of negatively charged trions this is possible by assigning spin-up to one electron and spin-down to the other one. With biexcitons we simply apply the same for the positive particles, also. The exciton-trion complex requires the account of Fermi statistics, which in this work is dealt with by the restricted path-integral Monte Carlo approach, and the free particle nodal restriction [27].

In this work the statistical standard error of the mean with 2σ limits is used as an error estimate for all observables from our PIMC simulations. Sampling in the configuration space is carried out using the Metropolis procedure [28] with multilevel bisection moves [29], and the thermal estimator [30] is used in the calculation of the total energy. We employ the PIMC method with the primitive approximation [30], for which we find that $T = 10$ K describes the ground states of our systems accurately, and that using Trotter number $M = 4000$ yields good balance between a feasible amount of computer time and accuracy. As the Trotter number M tends to infinity, the exact many-body results are obtained, but high accuracy is often found with reasonable values of M. More details are given in the Supplemental Material (SM) [24].

III. RESULTS

Before discussing the binding energies, it is useful to illustrate the spatial distribution of the electrons and holes in

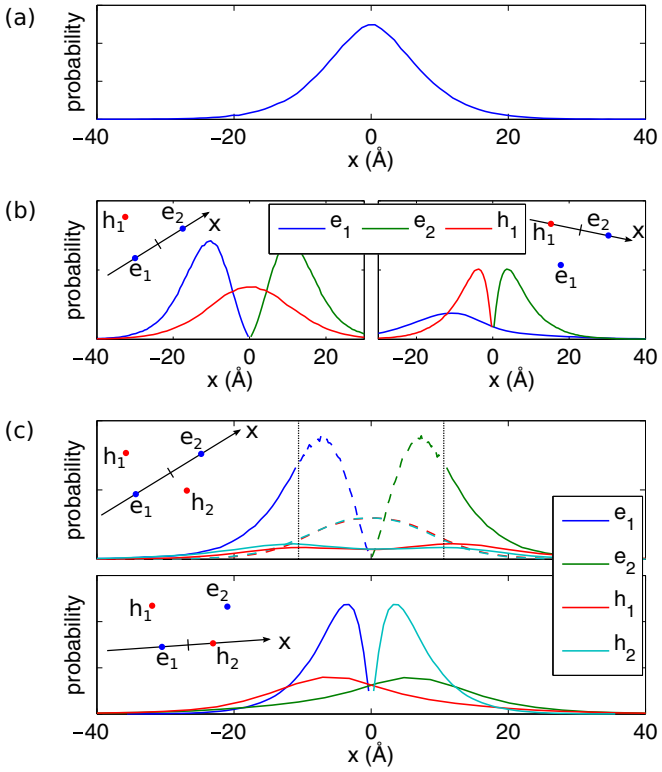

FIG. 2. (Color online) Particle coordinate distributions in the case of (a) exciton, (b) trion, and (c) biexciton. In (a), the hole is fixed at the origin. In (b) and (c), the x axis is chosen to pass along two particles as illustrated. Origin is at the center of mass of these two particles. In (c), the distributions for electron-electron distance larger (solid lines) and smaller (dashed lines) than 40 bohrs are distinguished.

these systems. In Fig. 2, we show the x-coordinate distribution of all particles, when the x axis is chosen to pass through two of the particles with the origin at their center of mass. In an exciton, the electron distribution when the hole is fixed at the origin is similar to that of the hydrogen $1s$ state, showing exponential decay at a larger distance. In the case of a negative trion, the hole is largely located between the electrons. When the distance between electrons in a biexciton is large, there is one hole located close to each electron [solid lines in Fig. 2(c)]. When the distance between electrons is small [dashed lines in Fig. 2(c)], the extent of the hole wave functions becomes too large to make such a distinction any more.

The root-mean-square (rms) averaged electron-hole separation for an exciton in suspended MoS_2 is found to be 11 Å, which is in agreement with previous model calculations [9,11] and with the GW+BSE calculated rms radius of 1 nm reported in Ref. [31]. The electron-electron rms separation for A^- is 29 Å and for the biexciton 23 Å (see SM for tabulated data of interparticle distances in all the considered TMDs [24]).

The binding energies for all complexes are given in Table II, together with the experimental results. Comparing the numbers over different materials, we observe that the binding energy depends strongly on the material polarizability χ_{2D}, but weakly on the effective masses. As a consequence, the results for A and B cases are generally very similar. For instance, even if the effective-mass ratio in WSe_2 differs by more than 30%, the binding energy differs by less than 5%. Our calculated results for B^- and B^+ trions and BB biexcitons were also very similar to the A counterpart and thus omitted from Table II. Finally, the effective-mass insensitivity also extends to negative and positive trions having nearly identical binding energies.

When comparing to the results obtained using the *ab initio* GW+BSE approach, as collected in Table II, our model tends to underestimate the exciton binding energies by $0.1 - 0.2$ eV; a satisfactory agreement. The difference can arise from the fairly small extent of the exciton wave function, and consequently the breakdown of the effective-mass approximation. There are no first-principles results available for comparison in the case of the trion, biexciton, or exciton-trion complex. Nevertheless, our results for excitons and trions are close to those obtained using the variational model for the case of $\kappa = 1$ [9], but clearly smaller than the estimate for the biexciton given in Ref. [6].

In experiments, TMD sheets are rarely suspended in vacuum. Dielectric environment has a strong effect on the screening of the interactions within the sheet and consequently on the binding energies [10–12,21,22]. The binding energies as a function of the average dielectric constant of the environment κ are shown in Fig. 3. For excitons, the dependence on κ can be fitted reasonably well with $E_b(\kappa = 1)/\kappa^\alpha$, when $\alpha \approx 0.7$ in agreement with the asymptotic form found in Ref. [22]. With increasing κ, the trion binding energy decreases faster than that of the biexciton and they are found equal at $\kappa \approx 4$. Since the short-range interaction is more strongly affected by the dielectric environment [cf. Fig. 1(c)], and considering the trion geometry shown in Fig. 2(b), the repulsive electron-electron interaction is affected less than the attractive electron-hole interaction. If the biexciton is approximated as two weakly bound excitons, then their binding energy should have only weak κ dependence.

Comparing our calculations to experimental results is hindered by the large variations in the reported numbers. Fortunately, however, many of these experiments are carried out with the TMD sheet placed on a SiO_2 substrate. Then, in order to facilitate the comparison we have recalculated all binding energies for $\kappa = 2$, approximately corresponding to a situation of SiO_2 on one side and vacuum/air on the other. The results are given in Table II. In the case of excitons, our calculated binding energies are now within 0.1 eV of the experimental values. For trions, our calculations are also generally in line with the experimental results or slightly underestimated as in the case of excitons. It is worth noting though, that some authors have reported similar binding energies for the A^- and A^+ trions [40] in agreement with our results, whereas others have found a larger binding energy for the A^- than for the A^+ [44,45].

In contrast to excitons and trions, which are commonly observed, the reports for biexcitons are very scarce. You *et al.* report a binding energy of 54 meV for both inter- and intravalley biexcitons in WSe_2 [6], Mai *et al.* report a binding energy of 70 meV for AA' biexciton (where A' denotes exciton in the K' valley) in MoS_2 [4], and Sie *et al.* found binding energy of 40 meV for the AB biexciton, and 60 meV for the AA' biexciton in MoS_2 [5]. These experimental results are clearly larger than our calculated values of about 20 meV.

TABLE II. Binding energies for all considered systems both in vacuum and in dielectric environment described by $\kappa = 2$. Experimental and computational results from literature are collected for comparison. Exciton energies are given in eV and binding energies of exciton complexes are given in meV. The 2σ statistical error estimate is given in parentheses for the PIMC results.

	MoS_2	$MoSe_2$	$MoTe_2$	WS_2	WSe_2
Exciton A	0.5265(2)	0.4769(2)	0.3752(2)	0.5098(2)	0.4564(2)
Exciton B	0.5339(2)	0.4853(2)	0.3828(2)	0.5309(2)	0.4777(2)
Other calc.	0.55 [32], 0.7 [22], 0.86 [10]	0.65 [33]		0.7 [34]	
Exciton A at $\kappa = 2$	0.3486(2)	0.3229(2)	0.2608(2)	0.3229(2)	0.2946(2)
Expt./Other calc.	0.43 [35,36], 0.46 [10]		0.58 [37]	0.32 [36]	0.37 [38]
Trion A^-	32.0(3)	27.7(3)	21.0(2)	33.1(3)	28.5(3)
Trion A^+	31.6(3)	27.8(3)	20.9(3)	33.5(4)	28.5(4)
Trion A^- at $\kappa = 2$	24.7(3)	22.1(3)	17.1(2)	24.3(3)	21.5(3)
Expt.	18 [39]	29 [40–42]	27 [37]	34 [43]	31 [42,44]
Biexciton AA	22.7(5)	19.3(5)	14.4(4)	23.9(5)	20.7(5)
Biexciton AA at $\kappa = 2$	20.3(5)	17.4(4)	12.9(4)	20.9(5)	18.1(4)
Ex+Trion AA^-	17.0(6)	16.4(5)	12.5(5)	14.9(6)	14.9(6)
Ex+Trion AA^- at $\kappa = 2$	13.5(4)	12.7(4)	10.0(4)	13.1(5)	12.2(4)

A likely explanation for the discrepancy is the neglect of exchange, and especially the electron-hole exchange, in our calculations. GW+BSE calculations yield a dark exciton 20 meV below the bright one [46,47], which originates from electron-hole exchange due to vanishing splitting of the conduction band in MoS_2. This is the exchange energy that should be added to our calculated value to yield the bright exciton energy. Neglect of exchange between electrons in a negative trion, i.e., setting their spins the opposite, inevitably leads to missing the exchange from one electron-hole pair, with the energy contribution similar to an exciton or smaller since the electron and hole are more separated. In the AA' biexciton there is no exchange between electrons or between holes, since they are assumed to have opposite spins. The electron-hole pairs at the K or K' valley should have similar electron-hole exchange contributions as excitons. However, if we consider that the electron at K is bound to the hole at K' and vice versa, these are dark excitons with no electron-hole exchange. Comparing such a configuration to the energies of two bright excitons that are missing exchange energies in our calculations leads to a total energy correction of 40 meV. Thus the obtained binding energy of 60 meV is then in line with the experimental values. Another explanation could be that in the experiment the biexcitons are bound to, e.g., impurities.

The only report of the exciton-trion complex, to the best of our knowledge, is in Ref. [41]. They deduced a binding energy of 4 ± 1.5 meV for $MoSe_2$ on SiO_2. Our number from Table II for this case is 12.7(4) meV, which is substantially larger.

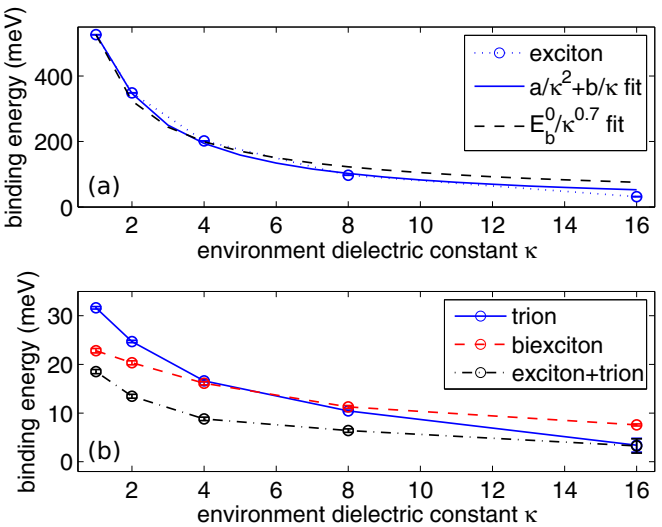

FIG. 3. (Color online) (a) Calculated exciton binding energies as a function of κ together with error bars (2σ). Dotted line is guide for the eye. Two fits are also shown: The coefficients for the first (solid line) are $a = -325$ meV and $b = 853$ meV. The second fit (dashed line) was proposed in Ref. [22]. (b) Binding energies and error bars for trion, biexciton, and exciton-trion complex as a function of κ.

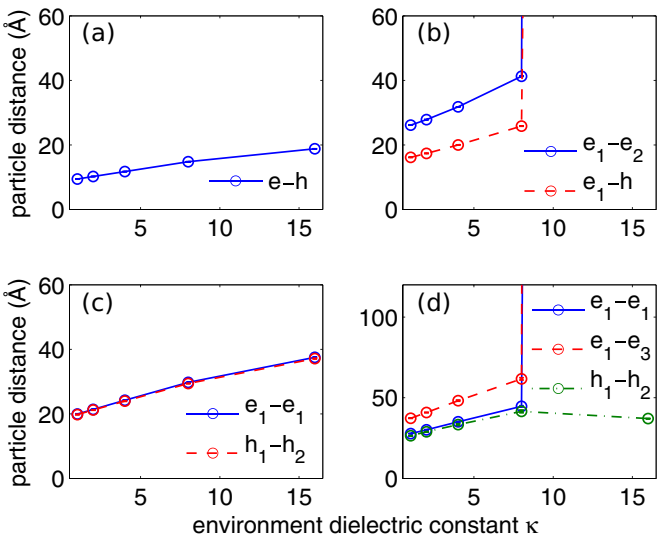

FIG. 4. (Color online) Selected average interparticle distances for exciton (a), trion (b), biexciton (c), and exciton-trion complex (d) in MoS_2 as a function of κ.

Finally, to illustrate the dependence of the system size on the environment, the interparticle distances as a function of κ are shown in Fig. 4. The particle distances generally scale linearly with κ. The trion and exciton-trion complex are found to dissociate after $\kappa > 8$. We note that the dissociation is facilitated by the nonzero temperature (10 K) used in our PIMC calculations. Interestingly, the exciton-trion complex does not dissociate to the exciton and trion, but to the biexciton (compare to $h_1 - h_2$ distance in biexciton) and a free electron. This is further confirmed by inspection of other particle-particle distances, i.e., electron-hole distances (not shown in the figure).

IV. CONCLUSIONS

In conclusion, we have studied excitons, trions, biexcitons, and exciton-trion complexes in two-dimensional transition metal dichalcogenides by an approach combining density functional theory with the quantum Monte Carlo method. We focused on the binding energies, interparticle separations, and on the role of the dielectric environment. Our approach reproduced exciton and trion properties in reasonably good agreement with experiment. We found that the larger complexes should also be stable with binding energies comparable to those of trions, although the relative stability can be controlled by the dielectric environment of the 2D sheet. Due to the large binding energies, environmental control, and coupling with the valley and spin indices of the material, we expect TMD materials to provide a versatile "laboratory" for studying, experimentally and theoretically, the physics of correlated many-body systems going even beyond the three-to-five-particle complexes considered here.

ACKNOWLEDGMENTS

We thank the Academy of Finland for the support under Projects No. 126205 (I.K.) and No. 263416 (H.P.K.), and through its Centres of Excellence Programme (2012-2017) under Project No. 251748 (H.P.K.). We also thank CSC-IT Center for Science Ltd. and Tampere Center for Scientific Computing for generous grants of computer time.

[1] K. F. Mak, C. Lee, J. Hone, J. Shan, and T. F. Heinz, Phys. Rev. Lett. **105**, 136805 (2010).
[2] K. F. Mak, K. He, J. Shan, and T. F. Heinz, Nat. Nanotechnol. **7**, 494 (2012).
[3] N. Kumar, S. Najmaei, Q. Cui, F. Ceballos, P. M. Ajayan, J. Lou, and H. Zhao, Phys. Rev. B **87**, 161403 (2013).
[4] C. Mai, A. Barrette, Y. Yu, Y. G. Semenov, K. W. Kim, L. Cao, and K. Gundogdu, Nano Lett. **14**, 202 (2014).
[5] E. J. Sie, A. J. Frenzel, Y.-H. Lee, J. Kong, and N. Gedik, Phys. Rev. B **92**, 125417 (2015).
[6] Y. You, X.-X. Zhang, T. C. Berkelbach, M. S. Hybertsen, D. R. Reichman, and T. F. Heinz, Nat. Phys. **11**, 477 (2015).
[7] L. V. Keldysh, JETP Lett. **29**, 658 (1979).
[8] P. Cudazzo, I. V. Tokatly, and A. Rubio, Phys. Rev. B **84**, 085406 (2011).
[9] T. C. Berkelbach, M. S. Hybertsen, and D. R. Reichman, Phys. Rev. B **88**, 045318 (2013).
[10] G. Berghäuser and E. Malic, Phys. Rev. B **89**, 125309 (2014).
[11] C. Zhang, H. Wang, W. Chan, C. Manolatou, and F. Rana, Phys. Rev. B **89**, 205436 (2014).
[12] A. Chernikov, T. C. Berkelbach, H. M. Hill, A. Rigosi, Y. Li, O. B. Aslan, D. R. Reichman, M. S. Hybertsen, and T. F. Heinz, Phys. Rev. Lett. **113**, 076802 (2014).
[13] B. Ganchev, N. Drummond, I. Aleiner, and V. Fal'ko, Phys. Rev. Lett. **114**, 107401 (2015).
[14] K. A. Velizhanin and A. Saxena, arXiv:1505.03910 [Phys. Rev. B (to be published)]; D. K. Zhang, D. W. Kidd, and K. Varga, Nano Lett. **15**, 7002 (2015); M. Z. Mayers, T. C. Berkelbach, M. S. Hybertsen, and D. R. Reichman, Phys. Rev. B **92**, 161404 (2015).
[15] D. A. Kleinman, Phys. Rev. B **28**, 871 (1983).
[16] A. Thilagam, J. Appl. Phys. **116**, 053523 (2014).
[17] I. Kylänpää, T. T. Rantala, and D. M. Ceperley, Phys. Rev. A **86**, 052506 (2012).
[18] N. M. Tubman, I. Kylänpää, S. Hammes-Schiffer, and D. M. Ceperley, Phys. Rev. A **90**, 042507 (2014).
[19] J. Tiihonen, I. Kylänpää, and T. T. Rantala, Phys. Rev. A **91**, 062503 (2015).
[20] L. Wirtz, A. Marini, and A. Rubio, Phys. Rev. Lett. **96**, 126104 (2006).
[21] H.-P. Komsa and A. V. Krasheninnikov, Phys. Rev. B **86**, 241201 (2012).
[22] Y. Lin, X. Ling, L. Yu, S. Huang, A. L. Hsu, Y.-H. Lee, J. Kong, M. S. Dresselhaus, and T. Palacios, Nano Lett. **14**, 5569 (2014).
[23] A. S. Rodin, A. Carvalho, and A. H. Castro Neto, Phys. Rev. B **90**, 075429 (2014).
[24] See Supplemental Material at http://link.aps.org/supplemental/10.1103/PhysRevB.92.205418 for further computational details, benchmarking of the interaction potential, and tabulated data of energies and particle distances for all considered exciton complexes.
[25] I. Hamada, Phys. Rev. B **89**, 121103 (2014).
[26] T. Björkman, J. Chem. Phys. **141**, 074708 (2014).
[27] D. M. Ceperley, J. Stat. Phys. **63**, 1237 (1991).
[28] N. Metropolis, A. W. Rosenbluth, M. N. Rosenbluth, A. H. Teller, and E. Teller, J. Chem. Phys. **21**, 1087 (1953).
[29] C. Chakravarty, M. C. Gordillo, and D. M. Ceperley, J. Chem. Phys. **109**, 2123 (1998).
[30] D. M. Ceperley, Rev. Mod. Phys. **67**, 279 (1995).
[31] D. Y. Qiu, F. H. da Jornada, and S. G. Louie, Phys. Rev. Lett. **111**, 216805 (2013).
[32] F. Hüser, T. Olsen, and K. S. Thygesen, Phys. Rev. B **88**, 245309 (2013).
[33] M. M. Ugeda, A. J. Bradley, S.-F. Shi, F. H. da Jornada, Y. Zhang, D. Y. Qiu, W. Ruan, S.-K. Mo, Z. Hussain, Z.-X. Shen *et al.*, Nat. Mater. **13**, 1091 (2014).
[34] Z. Ye, T. Cao, K. O'Brien, H. Zhu, X. Yin, Y. Wang, S. G. Louie, and X. Zhang, Nature (London) **513**, 214 (2014).
[35] C. Zhang, A. Johnson, C.-L. Hsu, L.-J. Li, and C.-K. Shih, Nano Lett. **14**, 2443 (2014).

[36] H. M. Hill, A. F. Rigosi, C. Roquelet, A. Chernikov, T. C. Berkelbach, D. R. Reichman, M. S. Hybertsen, L. E. Brus, and T. F. Heinz, Nano Lett. **15**, 2992 (2015).
[37] J. Yang, T. Lü, Y. W. Myint, J. Pei, D. Macdonald, J.-C. Zheng, and Y. Lu, ACS Nano **9**, 6603 (2015).
[38] K. He, N. Kumar, L. Zhao, Z. Wang, K. F. Mak, H. Zhao, and J. Shan, Phys. Rev. Lett. **113**, 026803 (2014).
[39] K. F. Mak, K. He, C. Lee, G. H. Lee, J. Hone, T. F. Heinz, and J. Shan, Nat. Mater. **12**, 207 (2013).
[40] J. S. Ross, S. Wu, H. Yu, N. J. Ghimire, A. M. Jones, G. Aivazian, J. Yan, D. G. Mandrus, D. Xiao, W. Yao *et al.*, Nat. Commun. **4**, 1474 (2013).
[41] A. Singh, G. Moody, S. Wu, Y. Wu, N. J. Ghimire, J. Yan, D. G. Mandrus, X. Xu, and X. Li, Phys. Rev. Lett. **112**, 216804 (2014).
[42] H. J. Liu, L. Jiao, L. Xie, F. Yang, J. L. Chen, W. K. Ho, C. L. Gao, J. F. Jia, X. D. Cui, and M. H. Xie, 2D Mater. **2**, 034004 (2015).
[43] B. Zhu, X. Chen, and X. Cui, Sci. Rep. **5**, 9218 (2015).
[44] A. M. Jones, H. Yu, N. J. Ghimire, S. Wu, G. Aivazian, J. S. Ross, B. Zhao, J. Yan, D. G. Mandrus, D. Xiao *et al.*, Nat. Nanotechnol. **8**, 634 (2013).
[45] J. S. Ross, P. Klement, A. M. Jones, N. J. Ghimire, J. Yan, M. G., T. Taniguchi, K. Watanabe, K. Kitamura, W. Yao *et al.*, Nat. Nanotechnol. **9**, 268 (2014).
[46] D. Y. Qiu, T. Cao, and S. G. Louie, Phys. Rev. Lett. **115**, 176801 (2015).
[47] H.-P. Komsa and A. V. Krasheninnikov, Phys. Rev. B **88**, 085318 (2013).